

Computational Study of Multistage Antiplasmodial Activity of Pentacyclic Triterpenoids and Their Derivatives

Innoent Onyesom^{1,*}, Ugochukwu E Uzuegbu¹, Chinwendu O. Elu¹, Evelyn T. Ojugbeli¹, Lisa I. Ekakitie¹, Jennifer E. Jaiyeoba-Ojigbo¹, Lilian E. Chris-Ozoko¹

¹ Malaria Research and Drug Discovery Unit, Department of Medical Biochemistry, Faculty of Basic Medical Sciences, Delta State University, Abraka, Nigeria; ionyesom@delsu.edu.ng (I.O.); ueuzuegbu@delsu.edu.ng (U.E.U.); eluchinwe@gmail.com (C.E.C); etojugebli@delsu.edu.ng (E.T.O); liekakitie@delsu.edu.ng (L.I.E.); ejaiyeoba@delsu.edu.ng (J.E.J.); lechrisozoko@delsu.edu.ng (L.E.C.);

* Correspondence: ionyesom@delsu.edu.ng;

Scopus Author ID 57729629200

Received: 30.03.2024; Accepted: 6.10.2024; Published: 15.02.2025

Abstract: Malaria is a highly infectious disease. Ongoing research focuses on novel plant-derived compounds for improved malaria treatment. This study explored the potential of various compounds to inhibit key proteins involved in the parasite's lifecycle. We analyzed the interaction between these compounds and parasite proteins through computational modeling and molecular docking. Our findings reveal several compounds with significant inhibitory activity against key proteins of parasite life stages. Compounds such as 3-Benzenesulfonyloxygen-5-22-diene-24-ethyl-cholesterol and P3 peptide exhibited high affinity for inhibiting PfCDPK1, essential for merozoite discharge and erythrocyte invasion. Purfalcamine and human p38 MAPK inhibitor drugs were effective in inhibiting Pfmap-2, which is vital for asexual reproduction. MMV009015 and MMV665796 compounds demonstrated significant inhibition of PfLPL3, crucial for asexual blood stage development. Purine and pyrimidine nucleosides were found to inhibit PFTMK. Moreover, our study identified compounds with inhibitory activity against proteins involved in other crucial processes of the parasite lifecycle, including sporozoite stage development, red blood cell invasion, and transmission-blocking proteins. Furthermore, certain compounds showed potential in modulating pathways associated with malaria severity and immune responses, indicating broader therapeutic implications. Therefore, this comprehensive analysis suggests that targeting specific proteins within the Plasmodium lifecycle with these compounds holds promise for developing effective antimalarial.

Keywords: malaria; PfCDPK1; pentacyclic triterpenoids; plasmodium falciparum; *Phyllanthus amarus*; proteins; RBC; sporozite; Pfmap-2.

© 2025 by the authors. This article is an open-access article distributed under the terms and conditions of the Creative Commons Attribution (CC BY) license (<https://creativecommons.org/licenses/by/4.0/>).

1. Introduction

Malaria, caused by parasites of the Plasmodium genus, is a life-threatening disease transmitted through the bite of infected female Anopheles mosquitoes [1]. It poses a significant global health challenge, especially in tropical and subtropical regions [2-4]. Symptoms of malaria typically include fever, chills, headache, muscle aches, fatigue, and nausea. If untreated, it can progress to severe illness, leading to complications such as organ failure and death [5]. Malaria is a complex disease involving various species of the Plasmodium genus [6]. The most severe form is caused by Plasmodium falciparum [7], while milder forms can be

caused by *Plasmodium vivax*, *Plasmodium malariae* [8], and *Plasmodium ovale* [9]. The infection process of malaria includes multiple stages and interactions between the parasite and the human host [10].

When a mosquito bites an infected person, it acquires Plasmodium parasites along with the blood. Inside the mosquito, these parasites undergo a complex development cycle, creating sporozoites in the mosquito's salivary glands. When an infected mosquito bites a human, it transfers sporozoites into the bloodstream through its saliva. These sporozoites quickly enter the human host and initiate the next phase of the infection. They travel to the liver, invade liver cells (hepatocytes), and undergo a series of transformations and multiplication, generating numerous merozoites [10].

Once matured, the merozoites are released from the liver cells and enter the bloodstream, infecting red blood cells (erythrocytes). Within the erythrocytes, the parasites continue to develop and replicate. Eventually, the infected erythrocytes rupture, releasing more merozoites into the bloodstream [11]. This invasion, replication, and rupture cycle leads to recurring episodes of fever and other malaria symptoms, including fever, chills, headache, muscle aches, fatigue, and nausea.

In some cases, particularly with *P. falciparum* infection, the disease can progress to severe malaria [12]. Severe malaria is characterized by complications such as organ failure, severe anemia, cerebral malaria (involving the brain), acute respiratory distress syndrome (ARDS), and renal failure [12,13].

Malaria treatment faces significant challenges, primarily due to drug resistance, limited treatment options, and inadequate access to healthcare and diagnostics [14,15]. Malaria parasites have developed resistance to commonly used antimalarial drugs, diminishing treatment effectiveness. Moreover, the number of effective antimalarial drugs is limited, and developing new drugs with different mechanisms of action is a slow and complex process [16].

In many malaria-endemic regions, accessing healthcare and appropriate treatment is hindered by remote locations, poor infrastructure, and financial constraints. Diagnostic challenges arise in resource-limited settings, where reliable tools for accurate diagnosis are scarce, leading to misdiagnosis or underdiagnosis [14,15].

Severe malaria cases, particularly those caused by *Plasmodium falciparum*, require specialized treatment and intensive care, but the lack of advanced healthcare facilities poses challenges. Moreover, the high treatment costs burden individuals and healthcare systems [17,18]. Addressing these limitations necessitates a comprehensive approach involving research for new drugs, improved healthcare access, enhanced diagnostics, better healthcare infrastructure, and strategies to combat drug resistance through surveillance and appropriate drug use.

Plants have long been used in traditional medicine systems to identify new antiviral and antimalarial drugs to treat various ailments, including malaria [19–21]. Many plant species contain bioactive compounds that possess antimalarial properties. These compounds can target the malaria parasites and inhibit their growth or kill them, relieving the infection. Some of these compounds include alkaloids [19], flavonoids [22], terpenoids [23], and quinones [24]. Notably, *Artemisia annua*, commonly known as sweet wormwood, has demonstrated remarkable efficacy against the malaria parasite, with the compound artemisinin and its derivatives serving as potent antimalarial drugs [25,26].

Phyllanthus amarus, a tropical plant from the Phyllanthaceae family, is known as Chanca Piedra, Stonebreaker, and Quebra Pedra. It is native to the Amazon rainforest and found

in regions like India, China, and the Caribbean [27]. This plant has a history of use in traditional medicine thanks to its bioactive compounds, such as alkaloids, flavonoids, lignans, and tannins. It is utilized for various conditions like urinary tract infections, kidney stones, jaundice, hepatitis B, and liver disorders [28]. *Phyllanthus amarus* and other plants like *Cinchona officinalis*, *Cryptolepis sanguinolenta*, Neem, and *Andrographis paniculata* have shown potential antimalarial activity. However, the effectiveness of plant-based remedies may not match modern antimalarial drugs, emphasizing the importance of standardization and quality control in their usage. Hence, *Phyllanthus amarus* can potentially yield multiple compounds that could serve as effective drugs against malaria infection.

The aim of this study is to evaluate the potential of specific compounds found in *Phyllanthus amarus* for their drug properties and their effectiveness against malaria. The compounds of interest include those found in the oil and solvent extract of *Phyllanthus amarus*. The study focuses on assessing the drug-likeness, ADME/Tox (absorption, distribution, metabolism, excretion/toxicity), QSAR (structure-activity/property relationship), physicochemical profile, and molecular docking of these compounds with specific protein targets in *Plasmodium falciparum*, the parasite causing malaria. By investigating the potential of these compounds, this study aims to contribute to developing novel antimalarial drugs.

2. Materials and Methods

2.1. Protein target selection.

Plasmodium falciparum's diverse protein requirements were addressed across the various stages of infection. The study focused on specific protein targets that are significant for multiple stages of the *P. falciparum* parasite. The UniProt database (<https://www.uniprot.org/>) and PlasmoDB (<https://plasmodb.org/plasmo/app>) were used to analyze each protein target thoroughly, as listed in Supplementary sheet 1 (Table S1).

2.2. 3D Structure prediction retrieval and domain analysis of proteins.

In addition to utilizing the AlphaFold Protein Structure Database (<https://alphafold.ebi.ac.uk/>), Robetta (<http://rosetta.bakerlab.org/>), OmegaFold (<https://github.com/omegafold/OmegaFold>), and SWISS-MODEL (<https://swissmodel.expasy.org/>) were also utilized to attain precise protein structure modeling. The computational platform Robetta, which the Baker laboratory developed, is highly regarded in the scientific community for its exceptional capabilities in protein structure prediction [1]. Similarly, OmegaFold, a freely available software for public use, gained significant attention due to its groundbreaking methodology in protein folding predictions [2]. The Swiss Institute of Bioinformatics maintains SWISS-MODEL, a reputable resource that offers high-quality homology modeling services [3]. By integrating various methodologies, we aimed to enhance the confidence of our structural predictions. The resulting three-dimensional conformations of the target proteins obtained through these databases are displayed in Supplementary Sheet 1 (Table S2).

Furthermore, domain analysis was performed for each target protein using the InterPro resource (<https://www.uniprot.org/>). This resource provided valuable information on the functional characteristics of the proteins, such as predicted domains and crucial binding sites.

2.3. Compounds selection and retrieval.

The compounds, namely Ursolic acid, Oleanolic acid, 3-O-Acetyloleanolic acid, Lupeol, Lupeol acetate, and stigmasterol, were retrieved from the PubChem (<https://pubchem.ncbi.nlm.nih.gov/>) database. PubChem, a widely used chemical information resource, is recognized as the most significant global repository for storing chemical compounds and their corresponding activities with various bioassays [4]. The National Centre for Biotechnology Information (NCBI) (<https://ncbi.nlm.nih.gov>) maintains the database and makes it accessible to the general public. The structures of the remaining listed compounds were created utilizing ChemDraw software as they were not publicly available on PubChem. ChemDraw is a popular chemical drawing software offering tools for drawing chemical structures, a name-to-structure translator, a chemical property database, a mass fragmentation tool, and 3D models. It facilitates efficient chemical database searches and query structures [5]. The compounds and the derivatives used in this study, along with their 2D structures, are mentioned in Supplementary Sheet 1 (Table S3). However, the compounds have been assigned labels to make their representation easier in the figures, as in Supplementary Sheet 1 (Table S3).

2.4. Virtual screening of *P. falciparum* multistage proteins against some pentacyclic triterpenoids and their derivatives.

According to this study, multistage proteins of *P. falciparum* were screened against stigmasterol, oleanolic-acid, lupeol, ursolic-acid, and their derivatives using Gnina (<https://github.com/gnina/gnina>). Gnina is a software based on deep learning techniques, explicitly utilizing an ensemble of convolutional neural networks, which serves as a scoring function for molecular docking [6]. Gnina features functionalities for scoring and optimizing ligands, and it has been reported to exhibit superior performance compared to the Autodock Vina software in the context of virtual screening [7]. Gina was employed for virtual screening by utilizing the protein structures and the structures of ursolic acid, oleanolic acid, lupeol, stigmasterol, and their derivatives in the “.PDB” format.

2.5. Molecular docking of *Plasmodium falciparum* antigens with host erythrocytes membrane surface receptors.

The HDOCK server (<http://hdock.phys.hust.edu.cn/>) is a comprehensive platform with tools for homology search, template-based modeling, structure prediction, macromolecular docking, integration of biological data, and job management, enabling reliable and quick protein-protein docking. Unlike other docking servers, the HDOCK server receives amino acid sequences as input and uses a hybrid docking strategy that includes experimental information about the protein-protein binding site and small-angle X-ray scattering during the docking and post-docking processes [8].

2.6. ADMET properties analysis.

In computational drug discovery, evaluating a compound's absorption, distribution, metabolism, excretion, and toxicity properties is essential to obtain a more comprehensive [9] understanding of its applicability as a potential drug [8]. The ADMET analysis was conducted for all the chosen ligands to accomplish this objective by utilizing their respective Simplified Molecular Input Line Entry System (SMILES) in the SwissADME online tool

(<http://www.swissadme.ch/>). SwissADME offers free access to an extensive pool of fast and robust predictive models for pharmacokinetics, physicochemical properties, and drug-likeness.

Lipinski and colleagues developed the "rule of five" to evaluate the drug-like properties and oral bioavailability of a compound to be administered as a drug. Based on the rule, the molecule should possess a molecular mass that does not exceed 500, a maximum of 5 hydrogen bond donors, a maximum of 10 hydrogen bond acceptors, and an octanol-water partition coefficient log P value that does not surpass 5 [10]. A molecule implied as a drug must not violate more than two of these rules. All the ligands under study showed a maximum of 0-2 Lipinski's violations and were used for further analysis.

2.7. Protein-ligand interaction analysis.

To study the protein-ligand interaction, Software PyMOL was used to make complex files for each docked protein in the *P. falciparum* parasite multistage proteins and their top-scoring ligands. Subsequently, the complex files underwent analysis using a web-based protein-ligand interaction profiler (PLIP) (<https://plip-tool.biotec.tu-dresden.de>) to identify the binding residues within the protein-ligand complexes. The PLIP tool accepts protein 3D structure as its input and facilitates the visualization of protein-ligand interactions [11]. Additionally, it generates a comprehensive report that includes details such as the name and position of the residues involved.

2.8. Molecular dynamics simulations.

Molecular dynamics simulations were performed on *P. falciparum* parasite multistage proteins to evaluate and compare their structural and functional disparities. The molecular dynamics simulations for the top docked complex of multistage parasite proteins were performed using Maestro 12.0 (version 12.2.012, Schrodinger, LLC, New York, NY).

The complexes were initially prepared using the protein preparation wizard, undergoing preprocessing and optimization by removing water molecules. The SPC water model was selected, and the process of structure minimization was carried out within the system builder. Ultimately, the molecular dynamics simulations were conducted at a temperature of 300K and a period of 25 nanoseconds.

3. Results and Discussion

3.1. *P. falciparum* sexual blood stage parasite (gametocytes) proteins.

In this study, 19 different proteins of the sexual blood stage of *P. falciparum* were screened against all compounds, and among these proteins, the compound 3-Benzenesulfonyloxygen-5-22-diene-24-ethyl-cholesterol showed the highest binding affinity of -11.01 kcal/mol with PfCDPK1 protein. However, the average score of this ligand with all proteins under study was found to be -8.84 kcal/mol, and this compound showed the least binding affinity of -6.03 kcal/mol with G377 protein. Considering other proteins of this stage, PfNek4 was found to be the second top-scoring protein and showed the highest binding affinity of -10.8 kcal/mol with the compound N-{3-[4-(3-(4-Hydroxybenzyl)-amino)-propyl]-piperaziny]-propyl}-3-O-acetylursolamine.

3.1.1. *P. falciparum* asexual blood stage parasite proteins.

The *P. falciparum* asexual blood stage parasite proteins contained 24 proteins. Among these proteins, the ligand 3-(2-4-dinitrophenyl)-5-22-diene-24-ethyl-cholesterol showed the highest binding affinity of -13.61 kcal/mol with PflPL3 protein. However, the average score of this ligand with all proteins under study was found to be -9.04 kcal/mol, and this compound showed the least binding affinity of -6.2 kcal/mol with G377 protein. Among this category, MT-CO1 showed the second highest binding affinity of -11.93 kcal/mol with its top ligand, 3-benzoyl-5-22-diene-24-ethyl-cholesterol.

3.1.2. *P. falciparum* skin stage parasite (sporozoite) proteins.

In total, 12 proteins related to *P. falciparum* skin stage parasite (Sporozoite) were utilized for screening against selected compounds. Among these proteins, the ligand Lupeol-acetylsalicylate showed the highest binding affinity of -10.78 kcal/mol with PKG protein. However, the average score of this ligand with all proteins under study was found to be -9.4 kcal/mol, and this compound showed the least binding affinity of 6.68 kcal/mol with G377 protein. Among this category, PfCDPK1 showed the highest binding affinity of -10.6 kcal/mol with 3-(3-carbonyl-pyridine)-5-22-diene-24-ethyl-cholesterol ligand.

3.1.3. *P. falciparum* liver stage parasite proteins.

A total of 12 proteins fall into the category of *P. falciparum* liver-stage parasite proteins. Among these proteins, the ligand 28-Methyl-3-trifluoroacetyl-oleanane showed the highest binding affinity -11.55 kcal/mol with the PMIV protein. However, the average score of this ligand with all proteins under study was found to be -9.03 kcal/mol, and this compound showed the least binding affinity of -6.15 kcal/mol with FabG. Among this category, FLN showed the highest binding affinity of -11.16 kcal/mol with 28-Methyl-3-trifluoroacetyl-oleanane ligand.

3.1.4. *P. falciparum* mosquito stage parasite proteins.

A total of six proteins in the category of *P. falciparum* mosquito stage parasite proteins. Among these proteins, the ligand Lupeol-acetylsalicylate showed the highest binding affinity -11.6 kcal/mol with PfGCS1 protein. However, the average score of this ligand with all proteins under study was found to be -9.42 kcal/mol, and this compound showed the least binding affinity of -6.68 kcal/mol with G377. Among this category, GEP1 showed the highest binding affinity of -11.52 kcal/mol with 28-Methyl-3-Oacetyloleanane ligand.

3.1.5. Transmission blocking proteins.

In total, 4 proteins (Pfs25, Pfs16, Pb51, and Plasmepsin V) related to the Transmission Blocking of *P. falciparum* were considered in this study. Among these proteins, the ligand 3-Trifluoroacetyloleanolic acid showed the highest binding affinity -9.97 kcal/mol with Pfs25 protein. However, the average score of this ligand with all proteins under study is -9.2 kcal/mol, and this compound showed the least binding affinity of -6.41 with G377. Among this category, Pfs16 showed the highest binding affinity of -9.72 kcal/mol with the trifluoroacetyl-oleanane ligand.

3.1.6. *P. falciparum* drug resistant proteins.

The *P. falciparum* drug-resistant proteins category contains 5 proteins. Among these proteins, the ligand Lupeol-isonicotinate showed the highest binding affinity -10.54 kcal/mol with PfCRT protein. However, the average score of this ligand with all proteins under study is -9.1 kcal/mol, and this compound showed the least binding affinity of -6.06 kcal/mol with G377 protein. Among this category, PfAp4AH showed the highest binding affinity of -9.57 kcal/mol with 3-(2-4-initrophenyl)-5-22-diene-24-ethyl-cholesterol ligands.

3.2. *P. falciparum* targets proteins to determine the ligands' mechanism of action.

Maurer's Cleft proteins were screened against stigmaterol, oleanolic acid, lupeol, ursolic acid, and their derivatives to determine the ligands' mechanism of action. Among Maurer's Cleft proteins, FIKK 10.1 showed the highest binding affinity of -11.8 kcal/mol with N-{3-[4-(3-(4-Hydroxybenzyl)-amino)-propyl]-piperazinyl]-propyl}-3-O-acetylursolamine ligand. However, the average score of this ligand with all proteins is -8.6 kcal/mol, and this compound showed the least binding affinity of -4.61 kcal/mol with PfEBA-175 protein. In total, 3 proteins (PfEMP1, RIFIN, and SURFIN) related to the *P. falciparum* immune evasion proteins were under study. Out of these 3 proteins, PfMP1 showed the highest binding affinity of -10.86 kcal/mol with the 3-O-Acetyl Oleanolic-acid compound. Furthermore, the average score of this ligand with all the proteins under study is -8.6 kcal/mol, and this ligand showed the least binding affinity, -5.91, with FabG protein.

3-Benzenesulfonyloxygen-5-22-diene-24-ethyl-cholesterol ligand showed the highest binding affinity of -10.63 kcal/mol with SERCA protein. However, the average score of this ligand 3-Benzenesulfonyloxygen-5-22-diene-24-ethyl-cholesterol with all the proteins is -8.8 kcal/mol and showed the least binding affinity of -6.03 kcal/mol with G377 protein. PfMQO protein showed the highest binding affinity of -10.25 kcal/mol with 28-Methyl-3-Oacetyloleanane ligand. Nevertheless, the average score of 28-Methyl-3-Oacetyloleanane ligand is -9.13 kcal/mol with all the proteins under examination, and this compound showed the least binding affinity of -6.08 kcal/mol with G377 protein.

Furthermore, *P. falciparum* antigens that interact with host erythrocyte membrane surface receptors include three proteins, namely PfEBA-175, PfEBL-1, and Rh5. Among these antigens, PfEBA-175 protein showed the highest binding affinity of -10.51 with N-{3-[4-(3-Ferrocenylamino)-propyl]-piperazinyl]-propyl}-3-O-acetylursolamide ligand. However, the average score of this ligand is -8.6 kcal/mol with all the proteins under study, and this compound showed the least binding affinity of -5.4 kcal/mol with LSA-1 protein. The binding affinities of all the top-scoring multistage proteins against their ligands are mentioned in Table 1. The surface view of the top complexes and surface view of antigens docked with their top-scoring compounds is provided in Figure 1.

Table 1. Each *P. falciparum* multistage protein against its top-scoring ligand and binding affinities.

Category	Protein	Compound	Affinity score
<i>P. falciparum</i> sexual blood stage parasite (gametocytes) proteins	PfCDPK 1	3-Benzenesulfonyloxygen-5-22-diene-24-ethyl-cholesterol	-11.01
<i>P. falciparum</i> asexual blood stage parasite proteins	PfLPL3	3-(2-4-dinitrophenyl)-5-22diene-24-ethyl-cholesterol	-13.61
<i>P. falciparum</i> skin stage parasite (sporozoite) proteins	PKG	Lupeol-acetylsalicylate	-10.78
<i>P. falciparum</i> liver stage parasite proteins	Plasmepsin IV	28-Methyl-3-trifluoroacetyl-oleanane	-11.55

Category	Protein	Compound	Affinity score
<i>P. falciparum</i> mosquito stage parasite proteins	PfGCS1	Lupeol-acetylsalicylate	-11.6
Transmission blocking proteins	Pfs25	3-Trifluoroacetyloleanolicacid	-9.97
<i>P. falciparum</i> drug resistant proteins	PfCRT	Lupeol-isonicotinate	-10.54
	PfAp4AH	3-(2,4-dinitrophenyl)-5,22-diene-24-ethyl cholesterol	-9.57
	PfHsp 70-1	Lupeol Acetylsalicylate	-9.49
	PfK13	28-methyl-3-trifluoroacetyloleanane	-8.49
	Multidrug resistance	3-Trifluoroacetyloleanolic acid	-8.06
<i>P. falciparum</i> target proteins to determine the ligands' mechanism of action			
Maurer's cleft distortion	FIKK10.1	N-{3-[4-(3-(4-Hydroxybenzyl)-amino)-propyl]-piperazinyl]-propyl}-3-O-acetylsolamine	-11.18
	FIKK9.1	Lupeol acetylsalicylate	-10.77
	PFE60/PIESP2	Lupeol acetylsalicylate	-10.02
<i>P. falciparum</i> immune evasion proteins	PfEMP1	3-O-Acetyloleanolic-acid	-10.86
	RIFIN	Lupeol acetylsalicylate	-9.51
	PfEMP1	3-O-Acetyloleanolic acid	-10.86
	SURFIN	3-O-Acetyloleanolic acid	-9.32
Disruption in Ca ²⁺ homeostasis	SERCA	3-Benzenesulfonyloxygen-5_22-diene-24-ethyl-cholesterol	-10.63
Disruption of <i>P. falciparum</i> mitochondrial membrane potential	PfMQO	28-Methyl-3-O-acetyl oleanane	-10.25
<i>P. falciparum</i> antigens with host erythrocytes membrane surface receptors	PfEBA-175	N-{3-[4-(3-Ferrocenylamino)--propyl]-piperazinyl]-propyl}-3-O-acetylsolamide	-10.51
Alteration of iRBC Surface tension for <i>P. falciparum</i> invasion	PfEBL-1	Lupeol acetylsalicylate	-9.58

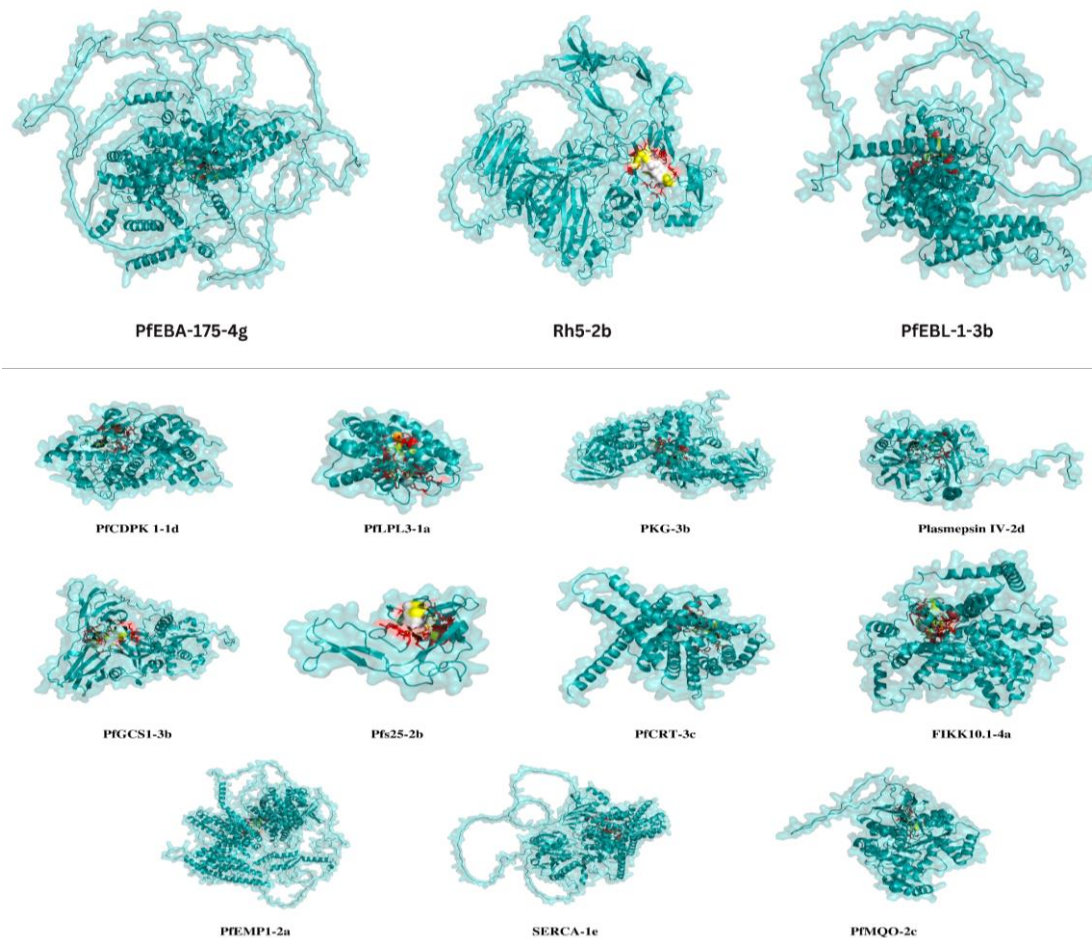


Figure 1. Surface view of *P. falciparum* antigens docked with their top-scoring ligands.

3.3. ADMET properties assessment of compounds.

During the initial assessment using SwissADME, the selected compounds were thoroughly evaluated for their absorption, distribution, metabolism, excretion, and toxicity properties. All compounds had less than three violations of Lipinski's rule, thus justifying their utilization in further investigations. The ADMET analysis of the compounds has been addressed in Table 2.

Table 2. ADMET of compounds.

Compounds	Molecular weight	LogP	HBA	HBD	TPSA	Lipinski's violations
3-Benzenesulfonyloxygen-5-22-diene-24-ethyl-cholesterol	552.865	9.214	3	0	43.37	2
3-(2-4-dinitrophenyl)-5-22-diene-24-ethyl-cholesterol	590.809	9.7244	6	1	110.67	2
Lupeol-acetylsalicylate	604.872	9.7464	5	0	61.83	2
28-Methyl-3-trifluoroacetyl-oleanane	524.752	9.362	2	0	26.3	2
3-Trifluoroacetyloleanolic acid	552.718	8.3468	3	1	63.6	2
Lupeol-isonicotinate	531.825	9.2845	3	0	39.19	2
28-Methyl-3-O-acetyloleanane	470.782	8.8196	2	0	26.3	1
N-{3-[4-(3-(4-Hydroxybenzyl)-amino)-propyl]-piperazinyl}-propyl-3-O-acetylsolamine	830.212	8.8302	8	2	117.05	2
3-O-Acetyloleanolic-acid	504.796	6.9022	4	3	69.92	2
N-{3-[4-(3-Ferrocenylamino)-propyl]-piperazinyl}-propyl-3-O-acetylsolamide	853.071	9.2854	6	2	73.91	2

3.4. Protein-ligand interaction assessment.

The protein-ligand interaction assessment was conducted to identify the interacting residues of top-scoring compounds with the docked proteins of each stage. Protein-ligand interaction analysis revealed distinct binding patterns among the top-scoring proteins. The PfCDPK1 protein interacted with the ligand 3-Benzenesulfonyl Oxygen-5-22-diene-24-ethyl-cholesterol at residue 60A (ARG) within the Protein kinase domain (56-325). PfEBA-175 protein demonstrated binding at residues 555A (GLY) and 591A (ASP) with the ligand N-{3-[4-(3-Ferrocenyl-Amine)-propyl]-piperazinyl}-propyl-3-O-acetazolamide. These interactions were found within the Duffy-antigen binding domain (486-640). In contrast, the PfEBA-175 interaction at residue 1267A (THR) was found outside the domain region.

Among the *P. falciparum* immune evasion proteins, PfEMP1 interacted with the ligand 3-O-Acetyl Oleanolic acid and displayed a diverse binding pattern. Residues 739A (TYR), 751A (TYR), and 1137A (THR) did not interact within any specific domain. Notably, residue 1681A (TYR) interacted within the Plasmodium falciparum erythrocyte membrane protein 1, acidic terminal segment (1631-2064) domain. The protein PfGCS1 exhibited binding at residue 14A (ARG) with the ligand Lupeol-acetylsalicylate within the Generative cell specific-1/HAP2 domain (9-543). Pfs25 displayed interactions at residue 89A (THR) with the ligand 3-Trifluoro Acetyl Oleanolic acid. These interactions were found within the Ookinete surface antigen, EGF domain (74-115), and EGF-like domain (74-115). Protein PKG interacted at residue 190A (ASN) with the ligand Lupeol-acetylsalicylate within the Cyclic nucleotide-binding domain (176-289). Additionally, it interacted at residue 714A (GLY) with the ligand Lupeol-acetylsalicylate within the Protein kinase domain (56-325).

Plasmepsin IV protein interacted at residue 200A (SER) with the ligand 28-Methyl-3-trifluoroacetyl-oleanane. These interactions were found within the Peptidase family A1 domain

(137-445) and the Pepsin-like domain (137-444). SERCA protein interacted with the ligand 3-Benzenesulfonyl Oxygen-5-22-diene-24-ethyl-cholesterol at residue 323A (THR), but the interaction did not occur within the domain region. The protein PfCRT formed interactions with the ligand Lupeol isonicotinate at residue 90A (SER); however, it does not have known domains through literature or protein databases.

Moreover, PflPL3 interacted with ligand 3-(2-4-dinitrophenyl)-5-22-diene-24-ethyl-cholesterol at 244A (SER), PfMQO interacted with ligand 28-Methyl-3-O-acetyl oleanane at multiple residues 441A (GLY), 117A (ASN), 369A (ASP), and FIKK10.1 interacted with ligand N-{3-[4-(3-(4-Hydroxybenzyl)-amino)-propyl]-piperazinyl}-propyl}-3-O-acetyl ursolamine at residue 305A (ASN). Neither of these proteins has any known domains, as shown by literature or protein databases.

The detailed information regarding the binding residues, amino acids, and their respective binding locations within the domain for top-scoring target protein at each stage is represented in Supplementary Sheet 1 (Table S4).

3.5. Molecular dynamic simulations.

The simulation results include diverse categories of *P. falciparum* parasite stages: sexual blood, asexual blood, skin (sporozoite), liver, and mosquito. Additionally, they involve various proteins related to transmission-blocking, drug resistance, Maurer's cleft, immune evasion, Sarco-endoplasmic reticulum Ca²⁺ ATPase, L-malate: quinone oxidoreductase, and *P. falciparum* antigens interacting with host erythrocyte membrane surface receptors. Top complexes within these categories, such as PfCDPK1-3-Benzenesulfonyl-Oxygen-5-22-diene-24-ethyl-cholesterol, PflPL3-3-(2-4-dinitrophenyl)-5-22-diene-24-ethyl-cholesterol, PKG-Lupeol-acetylsalicylate, Plasmeprin IV-28-Methyl-3-trifluoroacetyl-oleanane, PfGCS1-Lupeol-acetylsalicylate, Pfs25-3-Trifluoro-Acetyl-Oleanolic-Acid, PfCRT-Lupeol-isonicotinate, FIKK 10.1-N-{3-[4-(3-(4-Hydroxybenzyl)-amino)-propyl]-piperazinyl}-propyl}-3-O-acetylursolamine, PfEMP1-3-O-Acetyl-Oleanolic-acid, SERCA-3-Benzenesulfonyl Oxygen-5-22-diene-24-ethyl-cholesterol, PfMQO-28-Methyl-3-O-acetyl-oleanane, and PfEBA-175-N-{3-[4-(3-Ferrocenylamino)-propyl]-piperazinyl}-propyl}-3-Oacetylursolamide, demonstrated distinct RMSD values, for both the protein and ligand at the conclusion of the simulation, of 3.54 Å and 3.04 Å, 5.40 Å and 4.14 Å, 5.00 Å and 3.67 Å, 12.36 Å and 2.39 Å, 4.18 Å and 2.47 Å, 6.08 Å and 10.04 Å, 7.64 Å and 7.01 Å, 7.01 Å and 3.52 Å, 10.01 Å and 3.89 Å, 11.69 Å and 3.91 Å, 4.61 Å and 2.52 Å, and 22.49 Å and 7.93 Å, respectively (Figure 2a, b). Through simulation results, it was observed that overall the most stable complex was PfCDPK1-3-Benzenesulfonyl-Oxygen-5-22-diene-24-ethyl-cholesterol and the most unstable complex was PfEBA-175-N-{3-[4-(3-Ferrocenylamino)-propyl]-piperazinyl}-propyl}-3-Oacetylursolamide. Results of RMSF per residues protein sequence length (1-500), protein sequence length (500-1000), and protein sequence length (1000+) are illustrated in Figure 3 (a) (b) and (c), respectively. Additionally, the molecular dynamic simulation results of the radius of gyration over time, solvent available surface area of ligand over time, and polar surface area of ligand over time are shown in Figure 4 (a) (b) and (c), respectively. Moreover, the highest and lowest values of RMSF, the highest value of protein-ligand contacts, all the values of ligand-protein contacts, and the ligand properties of all top complexes are mentioned in Table 3.

Table 3. RMSF, Protein-ligand contacts, Values of ligand-protein contacts, and ligand properties of all top complexes.

Complexes	P-RMSF (Highest) (Å)	P-RMSF (Lowest) (Å)	P-L Contacts (Highest)	L-P Contacts (Interaction)	L-P Contacts (30%)	L-P Contacts (Interacted)	rGyr-range (Å)	SASA-range (Å ²)	PSA-range (Å ²)
PfCDPK1-1d	LYS-522 (4.30)	ILE-175 (0.41)	ARG-60 H-Bond = 0.394 Water Bridge = 0.272 Hydrophobic = 0.131	Yes	PHE-147	ARG-60 at 30%	5.38 - 6.47	156.60-336.25	69.37-90.50
PfLPL3-1a	LYS-4 (5.28)	VAL-245 (0.85)	ASN-275 H-Bond = 0.303 Water Bridge = 0.303	Yes	TRP-253		6.44 - 7.09	7.64 - 117.96	188.07-210.53
PKG-3b	GLU-228 (4.62)	PHE-600 (0.70)	ASN-190 H-Bond = 0.276 Water Bridge = 0.297	No			5.09-6.03	159.50-312.05	71.08-102.86
Plasmepsin IV-2d	GLY-25 (16.65)	ILE-244 (1.29)	TYR-313 Hydrophobic = 0.409	Yes	TYR-313		4.98-5.18	55.00-161.15	27.54-39.80
PfGCS1-3b	PRO-564 (6.78)	LEU-167 (5.34 Å)	ASN-481 Water Bridge = 0.527	Yes		GLU-411 at 30% ASN-481 at 43% through water	5.28-6.09	63.09-226.29	61.93-86.97
PfS25-2b	SER-154 (8.94)	CYS-98 (0.94)	THR-89 H-Bond = 0.483 Water Bridge = 0.203	Yes		THR-89 at 40%	4.85-5.17	169.29-440.57	90.08-110.46
PfCRT-3c	PHE-3 (11.36)	ILE-77 (0.89)	PHE-145 Hydrophobic = 0.532	Yes	PHE-145		5.18-5.54	53.07-162.96	43.63-59.49
FIKK 10.1-4a	LYS-37 (14.14)	THR-324 (0.67)	PHE-519 H-Bond = 0.612 Water Bridge = 0.208 Hydrophobic = 0.450	Yes	PHE-103	ASN-305 at 30% ARG-363 at 34 through water	7.26-8.41	32.35-193.27	158.98-188.00
PfEMP1-2a	HIS-437 (81.73)	ARG-111 (0.88)	LYS-746 Ionic-0.104 Water Bridge = 1.008	Yes		SER-1134 at 51% through water VAL-1135 43% through Na, 53%	4.87-5.15	84.06-272.97	93.94-111.08
SERCA-1d	SER-582 (17.16)	ASN-980 (0.96)	ASN-59 H-Bond = 0.130 Water Bridge = 0.207	No Interaction					
PfMQO-2c	GLY-28 (8.77)	PHE-472 (0.61)	ASP-369 H-Bond = 0.879			ASP-369 at 87%	4.92-5.14	63.09-277.25	29.89-42.07

Complexes	P-RMSF (Highest) (Å)	P-RMSF (Lowest) (Å)	P-L Contacts (Highest)	L-P Contacts (Interaction)	L-P Contacts (30%)	L-P Contacts (Interacted)	rGyr-range (Å)	SASA-range (Å ²)	PSA-range (Å ²)
PfEBA-175-4g	ARG-1214 (32.11)	SER-1216 (29.20 Å)	PHE-1265 Hydrophobic = 0.653 Water Bridge = 0.043		TYR-1358 TRP-594	HIS-1361 at 42% PHE-1265 at 45%	5.81-8.64	185.73-53-.22	54.14-98.77

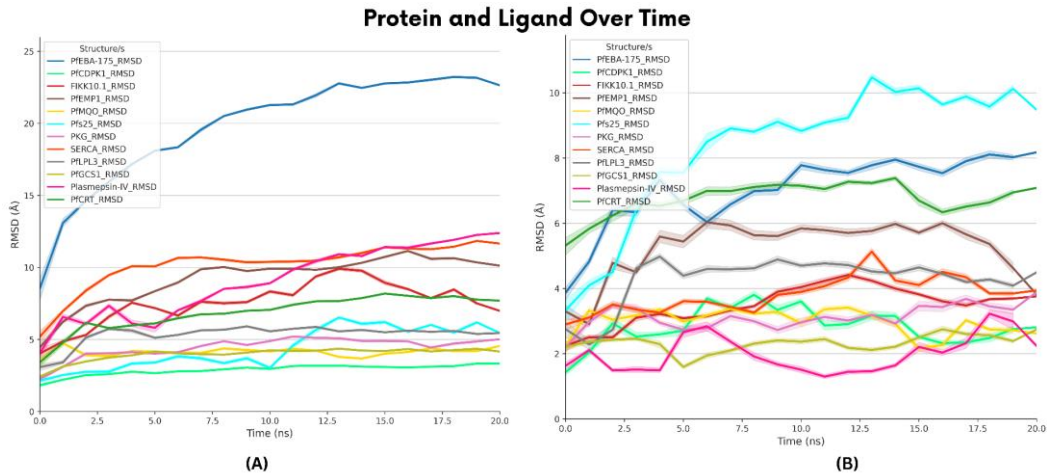


Figure 2. Molecular dynamics simulation results of all top proteins with their compounds performed on Maestro. (a) Protein RMSD; (b) Ligand RMSD.

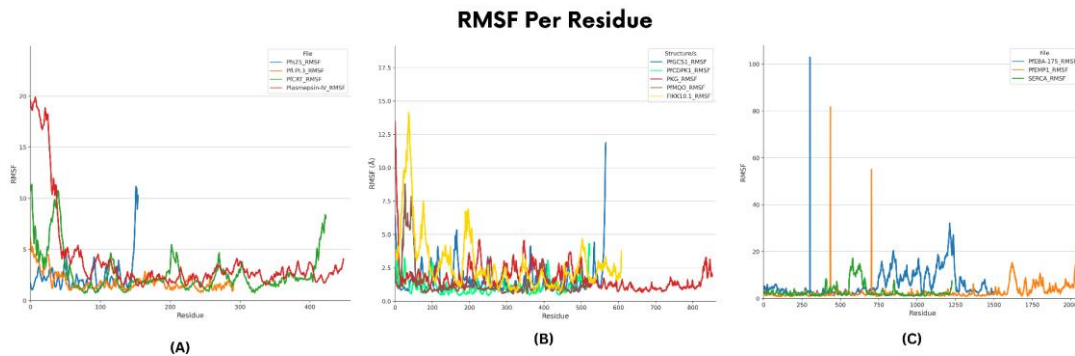


Figure 3. Results of RMSF Per Residues (a) Protein sequence length (1-500); (b) Protein sequence length (500-1000); (c) Protein sequence length (1000+).

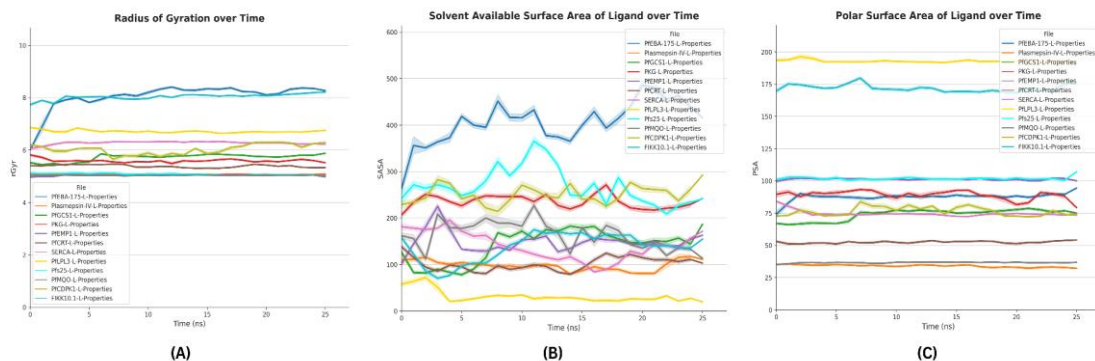


Figure 4. Molecular dynamic simulation results of (a) radius of gyration over time; (b) Solvent available surface area of ligand over time; (c) Polar surface area of ligand over time.

3.6. Discussions.

This study primarily focused on screening multistage proteins of *P. falciparum* against compound names and their derivatives to assess their impact on inhibiting these target proteins for therapeutic interventions in malaria. Furthermore, domain analysis and PLIP were performed to identify whether the ligand interacted within the functional domains of the target proteins. The results of virtual screening revealed that distinct ligands have distinct binding affinities for individual proteins in *P. falciparum* malarial parasite multistage proteins. Among the proteins related to the *P. falciparum* sexual blood stage of the parasite, PfCDPK1 was found to be inhibited with the highest binding affinity with the 3-Benzenesulfonyloxygen-5-22-diene-24-ethyl-cholesterol compound. According to a study conducted by Bansal *et al.*, (2013), the P3 peptide selectively inhibits the functional activity of PfCDPK1, preventing *P. falciparum* merozoites from discharging micronemes and invading erythrocytes. A previously discovered PfCDPK1 selective inhibitor, purfalcamine, also prevents microneme discharge and erythrocyte invasion, indicating PfCDPK1's function in this process. PfCDPK1 has been validated as a drug development target, and studies revealed that interfering with its molecular regulation may give a unique way to remove malaria parasite infections [13]. Another crucial protein, Pfmmap-2, is required for the completion of asexual reproduction and is thus a validated target for therapeutic intervention [14]. The rate of recombinant Pfmmap-2 autophosphorylation *in vitro* can be used to determine the inhibitory effect of human p38 MAPK inhibitor drugs on Pfmmap-2 [15]. Moreover, simulation results showed that the PfCDPK1-3-Benzenesulfonyloxygen-5-22-diene-24-ethyl-cholesterol complex was overall stable throughout the simulation time. However, our findings showed that 3-Benzenesulfonyloxygen-5-22-diene-24-ethyl-cholesterol and 3-Trifluoroacetyloleanolic acid compounds may inhibit PfCDPK1 and Pfmmap-2 proteins and may be used as antimalarial agents.

In *P. falciparum* asexual blood stage parasite proteins, the top protein PflLPL3 showed the highest binding affinity with 3-(2-(4-dinitrophenyl)-5-22-diene-24-ethyl-cholesterol) ligand. Interestingly, a study revealed that two compounds, MMV009015 and MMV665796, named PCB6 and PCB7, respectively, were discovered to decrease PflLPL3 enzyme activity by more than 70% at 5 μ M concentration. Both inhibitors were tested for effectiveness throughout the parasite's developmental cell cycle during asexual blood stages and provided profound outcomes [16]. Furthermore, PftMK can be inhibited by both purine and pyrimidine nucleosides, implying the possibility of selective PftMK inhibitors. The crystal structure of PftMK revealed the binding of both purine and pyrimidine nucleosides, indicating its utility as a novel therapeutic target [17]. Furthermore, it was observed through the simulation results that PflLPL3-3-(2-(4-dinitrophenyl)-5-22-diene-24-ethyl-cholesterol) complex was slightly unstable throughout the simulation time. However, our study showed that 3-(2-(4-dinitrophenyl)-5-22-diene-24-ethyl-cholesterol) and 3-Benzenesulfonyloxygen-5-22-diene-24-ethyl-cholesterol compounds may inhibit PflLPL3 and PftMK proteins respectively and can be used as antimalarial agents.

PKG, a cyclic GMP-dependent protein kinase, has been identified as the key molecular target responsible for 4-[2-(4-fluorophenyl)-5-(1-methylpiperidine-4-yl)-1H-pyrrol-3-yl]pyridine compound antiparasitic effect in *T. gondii* [18]. The PKG protein showed the highest binding affinity with Lupeol-acetylsalicylate ligand in *P. falciparum* skin stage parasite (sporozoite) proteins. 4-[2-(4-fluorophenyl)-5-(1-methylpiperidine-4-yl)-1H-pyrrol-3-yl]pyridine inhibits cGMP-induced protein kinase activity in biochemical fractions enriched for a

98 kDa protein identified using anti-PKG antisera. A study represented the initial effort to create innovative antimalarial substances by utilizing small-molecule inhibitors targeting a crucial interaction between parasite proteins necessary for invading red blood cells. The RON2 peptide fits snugly into AMA122's hydrophobic pocket and, if blocked by tiny compounds, could lead to potent new antimalarial therapy [19]. Moreover, this research showed that the compounds Lupeol-acetylsalicylate and Lupeol-acetate may inhibit the PKG and RON2 proteins and can be used as an antimalarial agent. Furthermore, our simulation results revealed that the PKG-Lupeol-acetylsalicylate complex exhibited a degree of instability throughout the simulation period.

In the *P. falciparum* liver stage parasite proteins category, Plasmepsin IV showed the highest binding affinity with the 28-Methyl-3-trifluoroacetyl-oleanane ligand. However, no evidence from the literature regarding the inhibition of this protein and its potential impact on malaria infection treatment was found. In the *P. falciparum* mosquito stage, parasite proteins lupeol-acetylsalicylate compound showed the highest binding affinity with the PfGCS1 protein. Among the *P. falciparum* mosquito stage parasite proteins, the top-scoring protein PfGCS1 was identified as a novel therapeutic target for antimalarial intervention, as lupeol-acetylsalicylate can inhibit this. This protein's inhibition may affect the gamete fusion function and male gametic expression [20]. No further literature evidence has been reported addressing the impact of inhibiting this protein in the context of malarial infection. However, our simulation results indicated that the Plasmepsin IV 28-Methyl-3-trifluoroacetyl-oleanane complex displayed a degree of high instability during the entire simulation period and, hence, can be used as a potential therapeutic strategy against malarial infection.

Pfs25 protein showed the highest binding affinity with 3 trifluoroacetyl oleanolic acid ligands in transmission-blocking proteins. Among the transmission-blocking proteins, the top-scoring protein Pfs25 was identified as a novel therapeutic target for antimalarial intervention as this can be inhibited by 3 trifluoroacetyl oleanolic acid. This inhibition may also affect the effectiveness of the Pfs25 vaccine, which is intended to elicit antibodies that suppress parasite development when anopheles mosquitoes consume it during blood meals [21].

In *P. falciparum* drug-resistant proteins, lupeol-isonicotinate showed the highest binding affinity with PfCRT protein. Among the *P. falciparum* drug-resistant proteins, PfCRT was identified as a novel therapeutic target for antimalarial intervention, as it can be inhibited by lupeol-isonicotinate. The inhibition of this protein may contribute to affecting the PfCRT chloroquine resistance through chloroquine exit from the digestive vacuoles of *P. falciparum*. Lupeol isonicotinate, acetate, and propionate proved to be the most potent compounds in stimulating the proliferation process of human skin cells. The findings suggest that modifying lupeol chemically leads to promising active compounds for treating skin injuries, such as thermal, chemical, and radiation burns [22]. Furthermore, as per the simulation results, the PfCRT-lupeol isonicotinate complex exhibited significant instability throughout the entire simulation duration. Furthermore, this research showed that the compound lupeol-isonicotinic may inhibit the PfCRT protein and can be used as an antimalarial agent.

The Maurer's Cleft protein category was virtually screened against the respective ligands to elucidate their mechanism of action. FIKK 10.1 showed the highest binding affinity with N-{3-[4-(3-(4-Hydroxybenzyl)-amino)-propyl]-piperazinyl]-propyl} -3-O-acetyl ursolamine ligand. The location of FIKK10.1 suggests that it may play an important role in the signaling pathways within the Maurer's cleft [23]. The specific function of FIKK Kinases in malaria parasites is unknown, but various studies have suggested a role in erythrocyte

remodeling [24]. The FIKK kinases are an accumulation of 18-26 serine-threonine kinases exported into the host cell by plasmodium parasites of the Laverania clade, which includes *P. falciparum* and other species infecting great apes [25]. However, in our study, N-{3-[4-(3-(4-Hydroxybenzyl)-amino)-propyl]-piperazinyl]-propyl}-3-O-acetyl compound may inhibit the FIKK 10.1 protein and may be used as an antimalarial agent. Moreover, based on the simulation results, the FIKK 10.1 complex involving N-{3-[4-(3-(4-Hydroxybenzyl)-amino)-propyl]-piperazinyl]-propyl}-3-O-acetylursolamine exhibited slight instability throughout the entirety of the simulation.

Among the *P. falciparum* immune evasion proteins, PfEMP1 showed the highest binding affinity with the 3-O-Acetyloleanolic acid ligand. *P. falciparum* erythrocyte membrane protein-1 (PfEMP-1) is a variable antigen secreted by the malaria parasite *P. falciparum*. PfEMP-1 interaction with the CD36 receptor on antigen-presenting cells regulates host immune responses. However, PfEMP-1 inhibits the early release of the cytokine interferon-gamma by specific immune cells after exposure to *P. falciparum* and specifically targets interferon-gamma production by gamma-delta-T, NK, and alpha beta-T cells, independent of the CD36 receptor. These findings highlight a malaria parasite-driven downregulation of the proinflammatory interferon-gamma response and the potency of transgenic parasites lacking PfEMP-1 as a valuable strategy for elucidating PfEMP-1 functions [26]. According to the simulation results, the PfEMP1 -3-O-Acetyloleanolic-acid complex displayed high instability throughout the entire simulation period. In our findings, the 3-O-Acetyloleanolic-acid compound may inhibit the PfEMP1 protein and may be used as an antimalarial agent.

SERCA-type Ca^{2+} -ATPase in the malarial parasite is considered a suitable molecular target for artemisinin. The spreading of antimalarial drug resistance now hinders the successful progress of eliminating malaria with artemisinin combination therapy [27]. In our study, amongst all ligands, 3-Benzenesulfonyl Oxygen-5-22-diene-24-ethyl-cholesterol showed the highest binding affinity with SERCA protein. Furthermore, the 3-Benzenesulfonyloxygen-5-22-diene-24-ethyl-cholesterol compound may inhibit the SERCA protein and may be used as an antimalarial agent.

A *P. falciparum* membrane protein, L-malate: quinone oxidoreductase (PfMQO), is an antimalarial drug target. However, little literature supports its expression and function information [29]. L-malate: quinone oxidoreductase (PfMQO) protein showed the highest binding affinity with 28-Methyl-3-O-acetyl oleanane ligand. However, our findings show that the 28-Methyl-3-O-acetyl oleanane compound may inhibit PMQO protein and may act as an antimalarial agent.

Targeting the invasion of red blood cells by *Plasmodium falciparum* is a promising strategy in the fight against malaria. *P. falciparum* EBA-175 (PfEBA-175) protein showed the highest binding affinity with N-{3-[4-(3-Ferrocenyl Amine)-propyl]-piperazinyl]-propyl}-3-O-acetyl ursolic amide ligand. During the invasion, PfEBA-175 interacts with the host receptor Glycophorin A (GypA) and is a potential candidate for a vaccine. Antibodies that identify PfEBA-175 have the potential to hinder parasite growth, although not all antibodies have this inhibitory effect. However, in our results, N-{3-[4-(3-Ferrocenyl Amine)-propyl]-piperazinyl]-propyl}-3-O-acetazolamide compound may inhibit PfEBA-175 protein and may be used as an antimalarial agent. Although these compounds might inhibit their inhibition of the interaction between the antigen and host receptor, the results revealed that it showed a prominent difference. Additionally, according to the simulation results, the PfEBA-175-N-{3-[4-(3-Ferrocenyl Amine)-propyl]-piperazinyl]-propyl}-3-O-acetyl ursolic amide complex displayed

pronounced instability throughout the entire simulation and therefore further research is required to establish the inhibition of this protein by natural compounds.

It is therefore concluded that various multistage proteins of *P. falciparum* pathogen and host play a crucial role in the development of malaria and how their inhibition via *Phyllanthus amarus*-derived natural compounds can be utilized as a potentially effective therapy against malaria.

4. Conclusions

The findings of this study emphasize the significance of targeting multistage proteins in *Plasmodium falciparum* using natural compounds derived from *Phyllanthus amarus* for malaria therapy. Through virtual screening and molecular interaction studies, promising candidates have been identified for inhibiting key proteins involved in parasite invasion, replication, immune evasion, and cytokine regulation. Compounds such as 3-Benzenesulfonyloxygen-5-22-diene-24-ethyl-cholesterol and Lupeol-acetylsalicylate exhibit notable binding affinities with target proteins, suggesting their potential as effective antimalarial agents. Simulation analyses further validate the stability and efficacy of these compound-protein complexes. This research highlights the importance of natural compounds in combating malaria and provides insights into novel therapeutic strategies for malaria treatment and prevention. Further studies are warranted to validate the efficacy and safety of these compounds in clinical settings and to elucidate their mechanisms of action for malaria therapy.

Funding

This research received no external funding.

Acknowledgments

We appreciate BioCode for the training on in silico methods and for the technical assistance rendered during the analysis.

Conflicts of Interest

The authors declare no conflict of interest.

References

1. Kim, D.E.; Chivian, D.; Baker, D. Protein structure prediction and analysis using the Robetta server. *Nucleic Acids Res.* **2004**, *32*, W526–W531, <https://doi.org/10.1093/nar/gkh468>.
2. Wu, R.; Ding, F.; Wang, R.; Shen, R.; Zhang, X.; Luo, S.; *et al.* High-resolution de novo structure prediction from primary sequence [Internet]. *bioRxiv* **2022**, p. 2022.07, <https://doi.org/10.1101/2022.07.21.500999>.
3. Waterhouse, A.; Bertoni, M.; Bienert, S.; Studer, G.; Tauriello, G.; Gumienny, R.; *et al.* SWISS-MODEL: homology modelling of protein structures and complexes. *Nucleic Acids Res.* **2018**, *46*, W296–W303, <https://doi.org/10.1093/nar/gky427>.
4. Kim, S.; Thiessen, P.A.; Bolton, E.E.; Chen, J.; Fu, G.; Gindulyte, A.; *et al.* PubChem Substance and Compound databases. *Nucleic Acids Res.* **2016**, *44*, D1202–D1213, <https://doi.org/10.1093%2Fnar%2Fgkv951>.
5. Mendelsohn, L.D. ChemDraw 8 Ultra, Windows and Macintosh Versions. *J. Chem. Inf. Comput. Sci.* **2004**, *44*, 2225–2226, <http://dx.doi.org/10.1021/ci040123t>.

6. McNutt, A.T.; Francoeur, P.; Aggarwal, R.; Masuda, T.; Meli, R.; Ragoza, M.; *et al.* GNINA 1.0: molecular docking with deep learning. *J Cheminformatics*. **2021**, *13*, 43, <https://doi.org/10.1186/s13321-021-00522-2>.
7. Sunseri, J.; Koes, D.R. Virtual Screening with Gnina 1.0. *Molecules* **2021**, *26*, 7369. <https://doi.org/10.3390/molecules26237369>.
8. Flores-Holguín, N.; Frau, J.; Glossman-Mitnik, D. Computational Pharmacokinetics Report, ADMET Study and Conceptual DFT-Based Estimation of the Chemical Reactivity Properties of Marine Cyclopeptides. *ChemistryOpen*. **2021**, *10*, 1142–1149, <https://doi.org/10.1002%2Fopen.202100178>.
9. Daina, A.; Michielin, O.; Zoete, V. SwissADME: a free web tool to evaluate pharmacokinetics, drug-likeness and medicinal chemistry friendliness of small molecules. *Sci Rep*. **2017**, *7*, 42717, <https://doi.org/10.1038/srep42717>.
10. Walters, W.P. Going further than Lipinski's rule in drug design. *Expert Opin Drug Discov*. **2012**, *7*, 99–107, <https://doi.org/10.1517/17460441.2012.648612>.
11. Salentin, S.; Schreiber, S.; Haupt, V.J.; Adasme, M.F.; Schroeder, M. PLIP: fully automated protein–ligand interaction profiler. *Nucleic Acids Res*. **2015**, *43*, W443–W447, <https://doi.org/10.1093/nar/gkv315>.
12. Openshaw, R. In vitro modelling of cellular haemozoin and inhibition by β -haematin inhibitors and their derivatives. Doctoral Thesis, University of Cape Town, South Africa, **2020**.
13. Bansal, A.; Singh, S.; More, K.R.; Hans, D.; Nangalia, K.; Yogavel, M.; *et al.* Characterization of Plasmodium falciparum Calcium-dependent Protein Kinase 1 (PfCDPK1) and Its Role in Microneme Secretion during Erythrocyte Invasion *. *J Biol Chem*. **2013**, *288*, 1590–1602, <https://doi.org/10.1074%2Fjbc.M112.411934>.
14. Camacho, L.R.; Ensergueix, D.; Perez, E.; Gicquel, B.; Guilhot, C. Identification of a virulence gene cluster of Mycobacterium tuberculosis by signature-tagged transposon mutagenesis. *Mol Microbiol*. **1999**, *34*, 257–267, <https://doi.org/10.1046/j.1365-2958.1999.01593.x>.
15. Brumlik, M.J.; Nkhoma, S.; Kiou, M.J.; Thompson, G.R.; Patterson, T.F.; Siekierka, J.J.; *et al.* Human p38 mitogen-activated protein kinase inhibitor drugs inhibit Plasmodium falciparum replication. *Exp Parasitol*. **2011**, *128*, 170–175, <https://doi.org/10.1016/j.exppara.2011.02.016>.
16. Sheokand, P.K.; Yamaro-Botté, Y.; Thakur, V.; Banday, M.M.; Asad, M.; Botté, C.Y.; Mohammed, A. A Plasmodium falciparum lysophospholipase regulates fatty acid acquisition for membrane biogenesis to enable schizogonic asexual division. *bioRxiv* **2021**, 07.01.450682, <https://doi.org/10.1101/2021.07.01.450682>.
17. Whittingham, J.L.; Carrero-Lerida, J.; Brannigan, J.A.; Ruiz-Perez, L.M.; Silva, A.P.G.; Fogg, M.J.; Wilkinson, A.J.; Gilbert, I.H.; Wilson, K.S.; González-Pacanowska, D. Structural basis for the efficient phosphorylation of AZT-MP (3'-azido-3'-deoxythymidine monophosphate) and dGMP by Plasmodium falciparum type I thymidylate kinase. *Biochem. J*. **2010**, *428*, 499–509, <https://doi.org/10.1042/BJ20091880>.
18. Diaz CA, Allocco J, Powles MA, Yeung L, Donald RGK, Anderson JW, *et al.* Characterization of Plasmodium falciparum cGMP-dependent protein kinase (PfPKG): Antiparasitic activity of a PKG inhibitor. *Mol. Biochem. Parasitol*. **2006**, *146*, 78–88, <https://doi.org/10.1016/j.molbiopara.2005.10.020>.
19. Srinivasan P, Yasgar A, Luci DK, Beatty WL, Hu X, Andersen J, *et al.* Disrupting malaria parasite AMA1- RON2 interaction with a small molecule prevents erythrocyte invasion. *Nat. Commun*. **2013**, *4*, 2261, <https://doi.org/10.1038/ncomms3261>.
20. Mori T, Hirai M, Kuroiwa T, Miyagishima S ya. The Functional Domain of GCS1-Based Gamete Fusion Resides in the Amino Terminus in Plant and Parasite Species. Berger F, editor. *PLOS ONE*. **2010**, *5*, e15957, <https://doi.org/10.1371/journal.pone.0015957>.
21. Scally, S.W.; McLeod, B.; Bosch, A.; Martin, S.R.; O'Dowd, V.; Luo, E.; Wu, L.; He, P.; Shakeri-Garakani, A.; Freeke, J.; *et al.* Molecular definition of multiple sites of antibody inhibition of malaria transmission-blocking vaccine antigen Pfs25. *Nat. Commun*. **2017**, *8*, 1568, <https://doi.org/10.1038/s41467-017-01924-3>.
22. Malinowska, M.; Miroslaw, B.; Sikora, E.; Ogonowski, J.; Wojtkiewicz, A.M.; Szaleniec, M.; *et al.* New lupeol esters as active substances in the treatment of skin damage. *PLOS ONE* **2019**, *14*, e0214216, <https://doi.org/10.1371/journal.pone.0214216>.
23. Jones, M.L.; Das, S.; Belda, H.; Collins, C.R.; Blackman, M.J.; Treeck, M. A versatile strategy for rapid conditional genome engineering using loxP sites in a small synthetic intron in Plasmodium falciparum. *Sci. Rep*. **2016**, *6*, 21800, <https://doi.org/10.1038/srep21800>.

24. Kats, L.M.; Fernandez, K.M.; Glenister, F.K.; Herrmann, S.; Buckingham, D.W.; Siddiqui, G.; *et al.* An exported kinase (FIKK4.2) that mediates virulence-associated changes in *Plasmodium falciparum*-infected red blood cells. *Int. J. Parasitol.* **2014**, *44*, 319-328, <https://doi.org/10.1016/j.ijpara.2014.01.003>.
25. Otto, T.D.; Rayner, J.C.; Böhme, U.; Pain, A.; Spottiswoode, N.; Sanders, M.; *et al.* Genome sequencing of chimpanzee malaria parasites reveals possible pathways of adaptation to human hosts. *Nat. Commun.* **2014**, *5*, 4754, <https://doi.org/10.1038/ncomms5754>.
26. D’Ombrain, M.C.; Voss, T.S.; Maier, A.G.; Pearce, J.A.; Hansen, D.S.; Cowman, A.F.; *et al.* *Plasmodium falciparum* Erythrocyte Membrane Protein-1 Specifically Suppresses Early Production of Host Interferon- γ . *Cell Host Microbe* **2007**, *2*, 130-138, <https://doi.org/10.1016/j.chom.2007.06.012>.
27. Nagasundaram, N.; George P.D.C.; Chiranjib C.; Karthick, V.; Thirumal K.D.; Balaji, V.; Siva, R.; Aiping L.; Zhang G.; Hailong Z. Mechanism of artemisinin resistance for malaria PfATP6 L263 mutations and discovering potential antimalarials: An integrated computational approach. *Sci. Rep.* **2016**, *6*, 30106, <https://doi.org/10.1038/srep30106>.
28. Eckstein-Ludwig, U.; Webb, R.J.; Van Goethem, I.D.A.; East, J.M.; Lee, A.G.; Kimura, M.; *et al.* Artemisinins target the SERCA of *Plasmodium falciparum*. *Nature* **2003**, *424*, 957-961, <https://doi.org/10.1038/nature01813>.
29. Ito, T.; Kajita, S.; Fujii, M.; Shinohara, Y. *Plasmodium* Parasite Malate-Quinone Oxidoreductase Functionally Complements a Yeast Deletion Mutant of Mitochondrial Malate Dehydrogenase. *Microbiol. Spectr.* **2023**, *11*, e00168-23, <https://doi.org/10.1128/spectrum.00168-23>.

Supplementary materials

Table S1. Selected protein targets reported for *P. falciparum* parasite multistage proteins.

P. falciparum sexual blood stage parasite (gametocytes) proteins		
Gene	Proteins	UniProt ID/PlasmoDB
PfNek 1	NIMA-related protein kinase	Q9NFP2
PfCDPK 7	Calcium-dependent protein kinase 7	PF3D7-1123100
PfNek 3	NIMA related kinase 3	Q8I629
PfCDPK 5	Calcium-dependent protein kinase 5	A0A5K1K8H0
PfCDPK 2	Calcium-dependent protein kinase 2	Q8ICR0
PfNek 2	NIMA related kinase 2	PF3D7-0525900
Pfppp1	Pf phosphoprotein phosphatase	A0A0L7KHD3
ZNF4	CCCH zinc finger protein	PF3D7-1134600
PfMAP2	Mitogen-activated protein kinase	Q9GR08
PfCDPK 3	Calcium-dependent protein kinase 3	Q9NJU9
PfHP1	<i>P. falciparum</i> heterochromatin protein 1	Pf7G8-2-000026400
PfCDPK 4	Calcium-dependent protein kinase 4	Q8IBS5
G377	Osmiophilic body protein	PF3D7-1250100
PfAP2-G	AP2 domain transcription factor	PF3D7-1222600
APC3	Anaphase-promoting complex 3	Anaphase-promoting complex 3
PfCDPK 1	Calcium-dependent protein kinase 1	P62343
PfCDPK 6	Calcium-dependent protein kinase 6	Q8IID5
MTRAP	Merozoite TRAP-like protein	PF3D7-1028700
PfNek 4	NIMA related kinase 4	C0H4N8
P. falciparum asexual blood stage parasite proteins		
Gene	Protein	UniProt ID/PlasmoDB
PfLPL3	<i>P. falciparum</i> lysophospholipase	Q8IE97
MT-CO1	Cytochrome C oxidoreductase	Q02766
TMK	Thymidylate synthetase	P13922
RPII	RNA Polymerase	P14248
MetRS	Methionyl-tRNA synthetase	A0A024V6Q4
TRXR	Thioredoxin reductase-2	P61076
MAHRP	Membrane associated histidine-rich protein	Q6V0X3
FP2B	Falcipain 2	Q56CY9
fabI	Type II fatty acid biosynthesis Fab I	Q965D5
MSP-1	Merozoite surface protein 1	P50495
MDH	Malate dehydrogenase	A0A1C3KZR0
GCS	Gamma glutamylcysteine synthetase	Q9TY17
PEPC	Phosphoenolpyruvate carboxylase	A0A1C3KF28
LDH	Lactate dehydrogenase	A0A1A8W5S5
CRK2	<i>Plasmodium falciparum</i> cyclin-dependent protein kinase	Q07785
LACZ	Hypoxanthine-guanine-xanthine phosphoribosyltransferase	P20035
PM4	Plasmepsin-2	Q816V3
TOP2	Topoisomerase II	P41001
TPI	Triosephosphate isomerase	Q07412
PMT	Phosphoethanolamine methyltransferase	Q6T755
fabH	Beta-ketoacyl-acyl carrier protein synthase III	O77078
EBA-175	Erythrocyte binding antigen 175	Q105A6
MSP2	Merozoite surface protein 2	P50498
FP3	Falcipain 3	Q9NB39
P. falciparum skin stage parasite (Sporozoite) proteins		
Gene	Protein	UniProt ID/PlasmoDB
PKG	cGAMP-dependent protein kinase	W7JX98

PfCDPK1	Plasmodium falciparum calcium-dependent protein kinase 1	P62343
B9	6-Cys-like protein	PF3D7-0317100
RON2	Rhoptry neck protein 2	Q8IKV6
CeLTOS	Cell-traversal protein for ookinetes and sporozoites	PF3D7-1216600
TREP	TREP - Adhesins Family Protein	A0A1C3L1T1
MyoA	Actin-myosin motor complex	Q8IDR3
CSP	Circumsporozoite protein	P02893
SIMP	Structural integrity maintenance protein	Q8IAY3
TLP	Adhesins Family Protein	A0A1Y3DJA5
TRAP	Adhesins Family Protein	P16893
LSA-1	Liver stage antigen 1	PF3D7-1036400
P. falciparum liver stage parasite proteins		
Gene	Protein	UniProt ID/PlasmoDB
FLN	Falcilysin	A0A0L7KF24
PMVII	Plasmepsin VII	A0A2I0BRF1
GFPT	Glucosamine-fructose-6-phosphate aminotransferase	A0A0L7K989
Pfa-SERA7	SERA cysteine protease 7	A0A0E4B233
FabG	β -oxoacyl-ACP reductase	Q965D6
Pfa-SERA2	SERA cysteine protease 2	A0A0E4B3F9
UCHL3	Ubiquitin carboxyl-terminal hydrolase	Q8IKM8
PM6	Plasmepsin VI	O77350
PM5	Plasmepsin V	Q8I6Z5
LISP2	Liver-specific protein 2	PF3D7-0405300
ClpQ	Heat shock protein hslv	Q8I5B6
PMIV	Plasmepsin IV	Q17SB3
P. falciparum mosquito stage parasite proteins		
Gene	Protein	UniProt ID/PlasmoDB
PfGCS1	Generative cell-specific 1	W8S2H7
GEP1	Gametogenesis essential protein 1	PF3D7-0515500
PLP4	Perforin like proteins 4	PF3D7-0819400
Pfs45-48	S48/45	Q26010
HAP2	Protein hapless 2	Q8IJQ3
PFS230	Gametocyte surface protein P230	P68874
P. falciparum transmission blocking proteins		
Gene	Protein	UniProt ID/PlasmoDB
Pfs25	Surface protein	A0A223LVT0
Pfs16	Parasitophorous vacuole membrane protein S16	Q6ZMA7
PMV	Plasmepsin V	Q8I6Z5
Pb51	Dolichyl-diphosphooligosaccharide--protein glycosyltransferase subunit OST3/OST6, putative	B9ZSI6
P. falciparum drug resistant proteins		
Gene	Protein	UniProt ID/PlasmoDB
PfCRT	Chloroquine resistance transporter	Q9N623
PfAp4AH	P. falciparum diadenosine tetraphosphate hydrolase	PF3D7-0520600
PfHsp 70-1	Heat shock protein 70	Q8IB24
PfK13 protein	Mutant Pfk13 protein	A0A1P8DAL1
PfMDR1	Multidrug resistance protein 1	A0A0D6E0Y6
P. falciparum target proteins to determine the ligands' mechanism of action		
Gene	Protein	UniProt ID/PlasmoDB
rex1	REX1 DNA repair protein	A0A060RT08
sbp1	Skeleton binding protein 1	Q9NFF5

mahrp1	Membrane-associated histidine-rich protein	Q6V0W8
mahrp2	Membrane associated histidine-rich protein	A0A060RXW0
Pf332	Antigen 332	Q7JXP5
GEXP07/CBP2	CX3CL1-binding protein 2	Q8IEJ0
PfEMP3	PfEMP3	A0A0L7K712
FIKK9.1	Serine/threonine protein kinase, FIKK family	A0A060RRM1
FIKK10.1	Serine/threonine protein kinase, FIKK family	A0A060RYE4
MAL7P1.172/PTP2	EMP1-trafficking protein	PF3D7_0731100
Pf1_00025	HNS binding protein	A0A2H4YGU4
Pf13_0076/PTP6	EMP1-trafficking protein	Q8IEI6/PF3D7_1302000
PFE60/PIESP2	Parasite-infected erythrocyte surface protein	PF3D7_0501200
FIKK12	Serine/threonine protein kinase, FIKK family	A0A060S0A4
pfmc-2tm	Pfmc-2TM Maurer's cleft two transmembrane protein	B9ZSJ3
semp1	Small exported membrane protein 1	PF3D7_0702400
RIFIN	Rifin	C0H4Q7
PfEMP1	Erythrocyte membrane protein 1, PfEMP1	Q8IBX0
SURFIN	Surfin	A0A0L7KEN7
SERCA	P-type Ca ²⁺ -transporting ATPase	Q5R2K6
PfMQO	Malate:quinone oxidoreductase	C6KT09
PfEBA-175	Erythrocyte binding antigen-175	Q8IBE8
PfEBL- 1	Erythrocyte binding ligand-1	A0A159SJ85
Rh5	Rh5-interacting protein	O97302
P. falciparum target proteins to determine the influence RBCs surface tension for plasmodium invasion		
IL-33	Interleukin-33	O95760
VAR2CSA	VAR2CSA	A0A0K2JP54
ST2	Interleukin-1 receptor-like 1	Q01638
IL-16	Pro-interleukin-16	Q14005
IL-2	Interleukin-2	P60568
IL-1A	Interleukin-1 alpha	P01583
IL-1B	Interleukin-1 beta	P01584
IL-13	Interleukin-13	P35225
IL-18	Interleukin-18	Q14116
IL-33	Interleukin-33	O95760
IL-11	Interleukin-11	P20809
IL-6	Interleukin-6	P05231
IL-10	Interleukin-10	P22301
IL-22	Interleukin-22	Q9GZX6
IL-4	Interleukin-4	P05112
IL-21	Interleukin	A0A224B028
IL-3	Interleukin-3	P08700
IL-5	Interleukin-5	P05113
IL-7	Interleukin-7	P13232
IL-8	Interleukin-8	P10145
IL-9	Interleukin-9	P15248
IL-15	Interleukin-15	P40933
IL-17A	Interleukin-17A	Q16552
IL-19	Interleukin-19	Q9UHD0
IL-20	Interleukin-20	Q9NYY1
IL-24	Interleukin-24	Q13007
IL-25	Interleukin-25	Q9H293
IL-26	Interleukin-26	Q9NPH9
IL-27	Interleukin-27 subunit alpha	Q8NEV9
IL-27B	Interleukin-27 subunit beta	Q14213
IL29	Interferon lambda-1	Q8IU54
IL30	Interleukin-27 subunit alpha	Q8NEV9
IL31	Interleukin-31	Q6EBC2
IL32	Interleukin-32	P24001
IL34	Interleukin-34	Q6ZMJ4
IL-12A	Interleukin-12 subunit alpha	P29459

IL-12B	Interleukin-12 subunit beta	P29460
IL-23A	Interleukin-23 subunit alpha	Q9NPF7
IL-28A	Interferon lambda-2	Q8IZJ0
IL-28B	Interferon lambda-3	Q8IZI9
IL-36A	Interleukin-36 alpha	Q9UHA7
IL-36B	Interleukin-36 beta	Q9NZH7
IL-14	Alpha-taxilin	P40222

Table S2. Selected protein targets and their accession IDs reported for *P. falciparum* parasite multistage proteins.

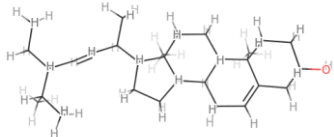
P. falciparum Sexual Blood Stage Parasite (gametocytes) Proteins	
Proteins	AlphaFold ID
NIMA-related protein kinase	AF-Q9NFP2-F1
Calcium-dependent protein kinase 7	AF-Q8IID2-F1
NIMA related kinase 3	AF-Q8I629-F1
Calcium-dependent protein kinase 5	AF-A0A5K1K8H0-F1
Calcium-dependent protein kinase 2	AF-Q8ICR0-F1
NIMA related kinase 2	AF-C0H4G2-F1
Pf phosphoprotein phosphatase	AF-A0A0L7KHD3-F1
CCCH zinc finger protein	AF-Q8II18-F1 (predicted through Robetta)
Mitogen-activated protein kinase	AF-Q9GR08-F1
Calcium-dependent protein kinase 3	AF-Q9NJU9-F1
<i>P. falciparum</i> heterochromatin protein 1	AF-Pf7G8-2-000026400-F1 (predicted through OmegaFold)
Calcium-dependent protein kinase 4	AF-Q8IBS5-F1
Osmiophilic body protein	No AlphaFold Structure (Predicted through SWISS-Model)
AP2 domain transcription factor	AF-Q8I5I9-F1 (Predicted through SWISS-Model)
Anaphase-promoting complex 3	AF-Q8I483-F1 (Predicted through OmegaFold)
Calcium-dependent protein kinase 1	AF-P62343-F1
Calcium-dependent protein kinase 6	AF-Q8IID5-F1 (predicted through Robetta)
Merozoite TRAP-like protein	AF-Q8IJB7-F1 (Predicted through OmegaFold)
NIMA related kinase 4	AF-C0H4N8-F1
P. falciparum Asexual Blood Stage Parasite Proteins	
Proteins	AlphaFold ID
<i>P. falciparum</i> lysophospholipase	AF-Q8IE97-F1
Cytochrome C oxidoreductase	AF-Q02766-F1
Thymidylate synthetase	AF-P13922-F1
RNA Polymerase	AF-P14248-F1
Methionyl-tRNA synthetase	AF-A0A024V6Q4-F1
Thioredoxin reductase-2	AF-P61076-F1
Membrane associated histidine-rich protein	AF-Q6V0X3-F1
Falcipain 2	AF-Q56CY9-F1
Type II fatty acid biosynthesis Fab I	AF-Q965D5-F1
Merozoite surface protein 1	AF-P50495-F1
Malate dehydrogenase	AF-A0A1C3KZR0-F1
Gamma glutamylcysteine synthetase	AF-Q9TY17-F1
Phosphoenolpyruvate carboxylase	AF-A0A1C3KF28-F1
Lactate dehydrogenase	AF-A0A1A8W5S5-F1
Plasmodium falciparum cyclin-dependent protein kinase	AF-Q07785-F1
Hypoxanthine-guanine-xanthine phosphoribosyltransferase	AF-P20035-F1
Plasmepsin-2	AF-Q816V3-F1
Topoisomerase II	AF-P41001-F1

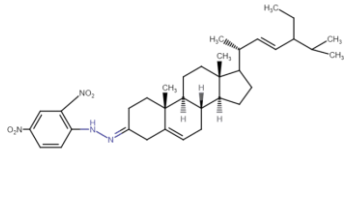
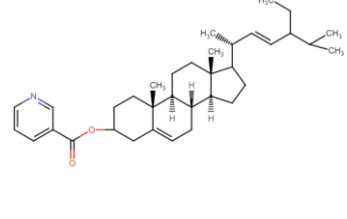
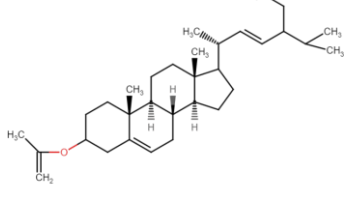
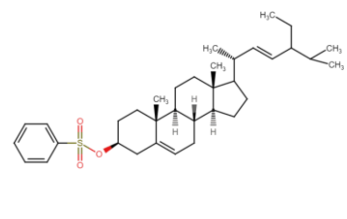
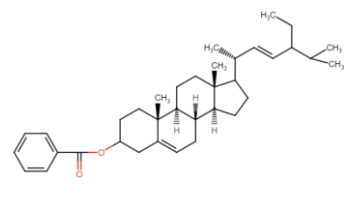
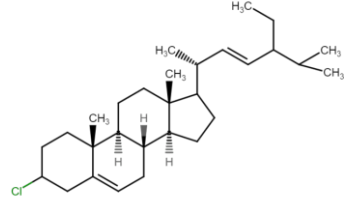
Triosephosphate isomerase	AF-Q07412-F1
Phosphoethanolamine methyltransferase	AF-Q6T755-F1
Beta-ketoacyl-acyl carrier protein synthase III	AF-O77078-F1
Erythrocyte binding antigen 175	AF-Q105A6-F1
Merozoite surface protein 2	AF-P50498-F1 (Predicted through OmegaFold)
Falcpain 3	AF-Q9NB39-F1
P. falciparum Skin Stage Parasite (Sporozoite) Proteins	
Proteins	AlphaFold ID
cGAMP-dependent protein kinase	AF-W7JX98-F1
Plasmodium falciparum calcium-dependent protein kinase 1	AF-P62343-F1
6-Cys-like protein	AF- C0H478-F1 (Predicted through Robetta)
Rhoptry neck protein 2	AF-Q8IKV6-F1
Cell-traversal protein for ookinetes and sporozoites	AF- Q8I5P1-F1 (Predicted through OmegaFold)
TREP - Adhesins Family Protein	AF-A0A1C3L1T1-F1
Actin-myosin motor complex	AF-Q8IDR3-F1
Circumsporozoite protein	AF-P02893-F1
Structural integrity maintenance protein	AF-Q8IAY3-F1
Adhesins Family Protein	AF-A0A1Y3DJA5-F1
Adhesins Family Protein	AF-P16893-F1
Liver stage antigen 1	AF- A0A143ZZD7-F1 (Predicted through Robetta)
P. falciparum Liver Stage Parasite Proteins	
Proteins	AlphaFold ID
Falcilysin	AF-A0A0L7KF24-F1
Plasmepsin VII	AF-A0A2I0BRF1-F1
Glucosamine-fructose-6-phosphate aminotransferase	AF-A0A0L7K989-F1
SERA cysteine protease 7	AF-A0A0E4B233-F1
Î²-oxoacyl-ACP reductase	AF- Q965D6-F1
SERA cysteine protease 2	AF-A0A0E4B3F9-F1
Ubiquitin carboxyl-terminal hydrolase	AF-Q8IKM8 -F1
Plasmepsin VI	AF-O77350-F1
Plasmepsin V	AF-Q8I6Z5-F1
Liver-specific protein 2	AF- Q8I1X6-F1 (Predicted through Robetta)
Heat shock protein hslv	AF-Q8I5B6-F1
Plasmepsin IV	AF-Q17SB3-F1
P. falciparum Mosquito Stage Parasite Proteins	
Proteins	AlphaFold ID
Generative cell-specific 1	AF-W8S2H7 -F1
Gametogenesis essential protein 1	AF- Q8I3V3-F1
Perforin like proteins 4	AF- Q8IB29-F1
S48/45	AF-Q26010 -F1
Protein hapless 2	AF-Q8IJQ3-F1
Gametocyte surface protein P230	No AlphaFold Structure (Predicted through SWISS-Model)
P. falciparum Transmission Blocking Proteins	
Proteins	AlphaFold ID
Surface protein	AF-A0A223LVT0 -F1
Parasitophorous vacuole membrane protein S16	AF-Q6ZMA7 -F1 (Predicted through OmegaFold)
Plasmepsin V	AF-Q8I6Z5-F1
Dolichyl-diphosphooligosaccharide--protein glycosyltransferase subunit OST3/OST6, putative	AF-B9ZSI6-F1
P. falciparum Drug Resistant Proteins	

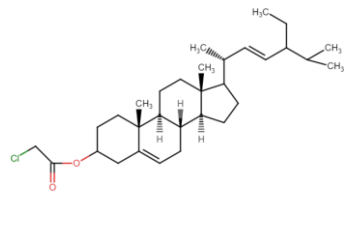
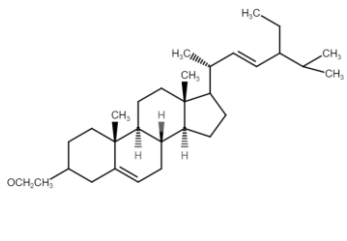
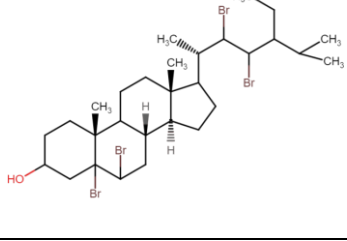
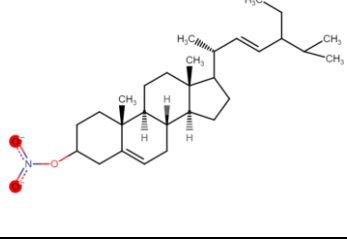
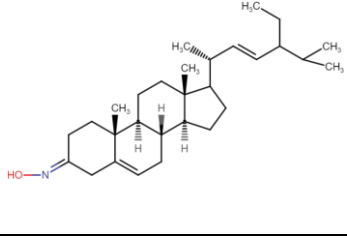
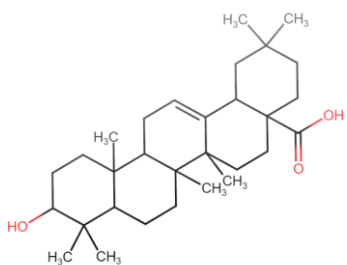
Proteins	AlphaFold ID
Chloroquine resistance transporter	AF-Q9N623 -F1
<i>P. falciparum</i> diadenosine tetraphosphate hydrolase	AF- C0H4F3-F1
Heat shock protein 70	AF-Q8IB24-F1
Mutant Pfk13 protein	AF-A0A1P8DAL1 -F1
Multidrug resistance protein 1	AF-A0A0D6E0Y6 -F1 (Predicted through OmegaFold)
<i>P. falciparum</i> target proteins to determine the ligands' mechanism of action	
Proteins	AlphaFold ID
REX1 DNA repair protein	AF-A0A060RT08-F1 (Predicted through OmegaFold)
Skeleton binding protein 1	AF-Q9NFF5-F1 (Predicted through OmegaFold)
Membrane-associated histidine-rich protein	AF-Q6V0W8-F1 (Predicted through OmegaFold)
Membrane associated histidine-rich protein	AF-A0A060RXW0-F1 (Predicted through OmegaFold)
Antigen 332	AF-Q7JPX5-F1 (Predicted through OmegaFold)
CX3CL1-binding protein 2	AF-Q8IEJ0-F1 (Predicted through OmegaFold)
PfEMP3	No AlphaFold Structure (Predicted through OmegaFold)
Serine/threonine protein kinase, FIKK family	AF-A0A060RRM1-F1 (Predicted through OmegaFold)
Serine/threonine protein kinase, FIKK family	AF-A0A060RYE4-F1 (Predicted through OmegaFold)
EMP1-trafficking protein	AF-Q8IBF1-F1 (Predicted through OmegaFold)
HNS binding protein	No AlphaFold Structure (Predicted through OmegaFold)
EMP1-trafficking protein	AF-Q8IEI6-F1 (Predicted through OmegaFold)
Parasite-infected erythrocyte surface protein	AF-Q8I488-F1 (Predicted through OmegaFold)
Serine/threonine protein kinase, FIKK family	AF-A0A060S0A4-F1 (Predicted through OmegaFold)
Pfmc-2TM Maurer's cleft two transmembrane protein	AF-B9ZSJ3-F1
Small exported membrane protein 1	AF-Q8IC43-F1 (Predicted through OmegaFold)
Rifin	AF-C0H4Q7-F1
Erythrocyte membrane protein 1, PfEMP1	AF-Q8IBX0-F1
Surfin	AF-A0A0L7KEN7-F1
P-type Ca ²⁺ -transporting ATPase	AF-Q5R2K6-F1
Malate:quinone oxidoreductase	AF-C6KT09-F1
Erythrocyte binding antigen-175	AF-Q8IBE8-F1
Erythrocyte binding ligand-1	AF-A0A159SJ85-F1
Rh5-interacting protein	AF-O97302-F1
<i>P. falciparum</i> Interleukin Proteins	
Pro-interleukin-16	AF-Q14005-F1
Interleukin-2	AF-P60568-F1
Interleukin-1 alpha	AF-P01583-F1
Interleukin-1 beta	AF-P01584-F1
Interleukin-13	AF-P35225-F1
Interleukin-18	AF-Q14116-F1
Interleukin-33	AF-O95760-F1
Interleukin-11	AF-P20809-F1
Interleukin-6	AF-P05231-F1
Interleukin-10	AF-P22301-F1

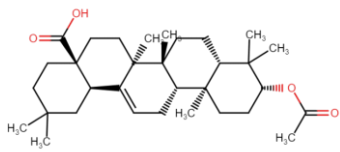
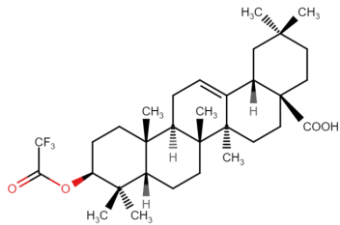
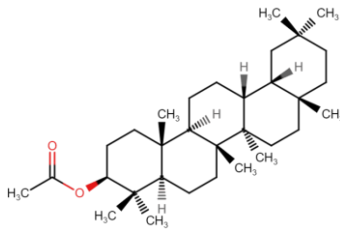
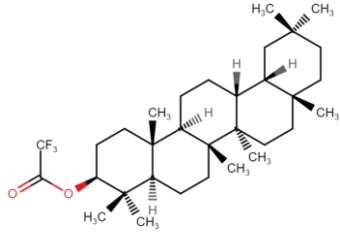
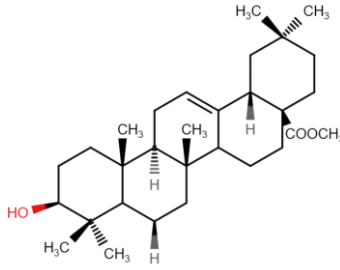
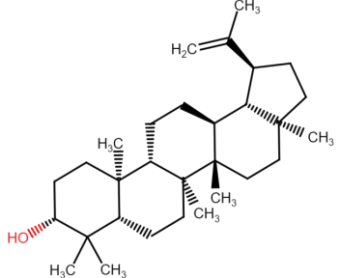
Interleukin-22	AF-Q9GZX6-F1
Interleukin-4	AF-P05112-F1
Interleukin	AF-A0A224B028-F1
Interleukin-3	AF-P08700-F1
Interleukin-5	AF-P05113-F1
Interleukin-7	AF-P13232-F1
Interleukin-8	AF-P10145-F1
Interleukin-9	AF-P15248-F1
Interleukin-15	AF-P40933-F1
Interleukin-17A	AF-Q16552-F1
Interleukin-19	AF-Q9UHD0-F1
Interleukin-20	AF-Q9NYY1-F1
Interleukin-24	AF-Q13007-F1
Interleukin-25	AF-Q9H293-F1
Interleukin-26	AF-Q9NPH9-F1
Interleukin-27 subunit alpha	AF-Q8NEV9-F1
Interleukin-27 subunit beta	AF-Q14213-F1
Interferon lambda-1	AF-Q8IU54-F1
Interleukin-27 subunit alpha	AF-Q8NEV9-F1
Interleukin-31	AF-Q6EBC2-F1
Interleukin-32	AF-P24001-F1
Interleukin-34	AF-Q6ZMJ4-F1
Interleukin-12 subunit alpha	AF-P29459-F1
Interleukin-12 subunit beta	AF-P29460-F1
Interleukin-23 subunit alpha	AF-Q9NPF7-F1
Interferon lambda-2	AF-Q8IZJ0-F1
Interferon lambda-3	AF-Q8IZI9-F1
Interleukin-36 alpha	AF-Q9UHA7-F1
Interleukin-36 beta	AF-Q9NZH7-F1
Alpha-taxilin	AF-P40222-F1
Plasmodium sequestration in brain	
Interleukin-33	AF-O95760-F1
Interleukin-1 receptor-like 1	AF-Q01638-F1
Plasmodium sequestration in placenta	
VAR2CSA	AF-A0A0K2JP54-F1

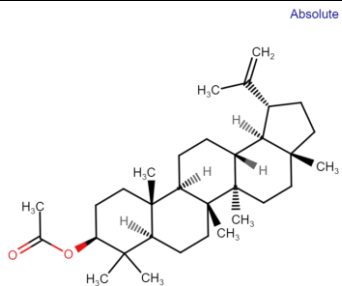
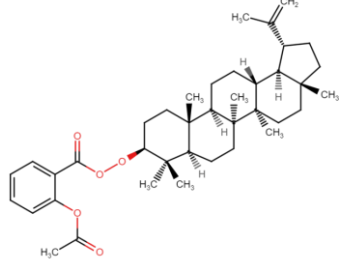
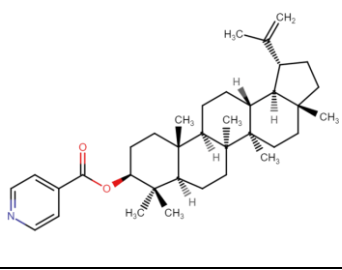
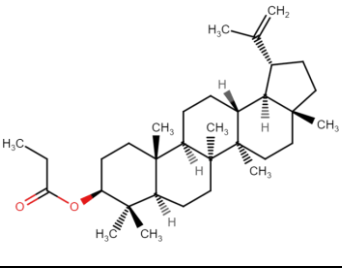
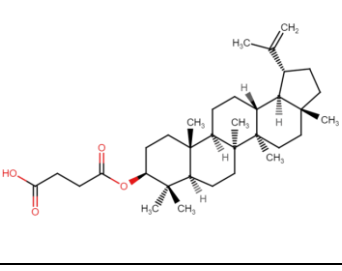
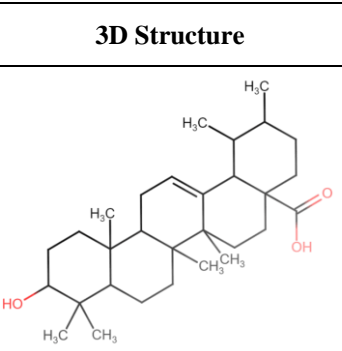
Table S3. Selected compounds and their derivative to target *P. falciparum* parasite multistage proteins.

Stigmasterol and Derivatives			
Name	Designated Label	Retrieval	3D Structure
Stigmasterol	1	PubChem ID: 5280794	

3-(2-4-dinitrophenyl)-5-22-diene-24-ethyl-cholesterol	1a	ChemDraw	
3-(3-carbonyl-pyridine)-5-22-diene-24-ethyl-cholesterol	1b	ChemDraw	
3-acetoxy-5-22-diene-24-ethyl-cholesterol	1c	ChemDraw	
3-Benzenesulfonyloxygen-5-22-diene-24-ethyl-cholesterol	1d	ChemDraw	
3-benzoyl-5-22-diene-24-ethyl-cholesterol	1e	ChemDraw	
3-chlorine-5-22-diene-24-ethyl-cholesterol	1f	ChemDraw	

3-chloroacetoxy-5-22-diene-24-ethyl-cholesterol	1g	ChemDraw	
3-Ethoxy-5-22-diene-24-ethyl-cholesterol	1h	ChemDraw	
3-hydroxyl-5-6-22-23-tetrabromo-24-ethyl-cholesterol	1i	ChemDraw	
3-nitro-5-22-diene-24-ethyl-cholesterol	1j	ChemDraw	
3-oximido-5-22-diene-24-ethyl-cholesterol	1k	ChemDraw	
Oleanolic acid and derivatives			
Name	Designated Label	Retrieval	3D Structure
Oleanolic-Acid	2	PubChem ID: 10494	

3-O-Acetyloleanolic-acid	2a	PubChem ID: 151202	
3-Trifluoroacetyloleanolicacid	2b	ChemDraw	
28-Methyl-3-O-acetyloleanane	2c	ChemDraw	
28-Methyl-3-trifluoroacetyl-oleanane	2d	ChemDraw	
28-Methoxyoleanolic-acid	2e	ChemDraw	
Lupeol and derivatives			
Name	Designated Label	Retrieval	3D Structure
Lupeol	3	PubChem ID: 259846	

Lupeol-acetate	3a	PubChem ID: 92157	
Lupeol-acetylsalicylate	3b	ChemDraw	
Lupeol-isonicotinate	3c	ChemDraw	
Lupeol-propionate	3d	ChemDraw	
Lupeol-succinate	3e	ChemDraw	
Ursolic Acid and derivatives			
Name	Designated Label	Retrieval	3D Structure
Ursolic-acid	4	PubChem ID: 64945	

N-{3-[4-(3-(4-Hydroxybenzyl)-amino)-propyl]-piperazinyl]-propyl}-3-O-acetylursolamine	4a	ChemDraw	
N-{3-[4-(3-(Bis(4-hydroxybenzyl)amino)propyl)piperazinyl]propyl}-3-O-acetylursolamide	4b	ChemDraw	
N-{3-[4-(3-(Bis(cyclopropylmethyl)amino)propyl)piperazinyl]propyl}-3-O-acetylursolamide	4c	ChemDraw	
N-{3-[4-(3-(Bispropylamino)-propyl)-piperazinyl]-propyl}-3-O-acetylursolamide	4d	ChemDraw	
N-{3-[4-(3-Aminopropyl)-piperazinyl]-propyl}-3-O-acetylursolamide	4e	ChemDraw	
N-{3-[4-(3-aminopropyl)-piperazinyl]-propyl}-ursolamide	4f	ChemDraw	
N-{3-[4-(3-Ferrocenylamino)-propyl]-piperazinyl]-propyl}-3-O-acetylursolamide	4g	ChemDraw	

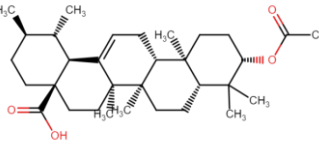
3-O-acetyl ursolic acid	4h	ChemDraw	
-------------------------	----	----------	---

Table S4. Binding residues of top-scoring target proteins of each stage with respective domains.

Protein Names	Ligands	Residue	Amino Acid	Domain of Interaction
IL10	3-benzoyl-5-22-diene-24-ethyl-cholesterol	162	GLU	No Domains
IL-5	Ursolic-acid	104A, 108A	LYS, GLU	No Domains
IL-25	28-Methyl-3-trifluoroacetyl-oleanane	63A	GLU	No Domains
IL-27	N-3-4-3-Aminopropyl-piperazinyl-amino-propyl-3-O-acetylursolamide	34A, 35A, 35A	GLY, ARG, ARG	No Domains
IL-28B	3-Trifluoroacetyloleanolicacid	75A, 76A, 76A	LEU, PHE, PHE	No Domains
IL-12B	N-3-4-3-Ferrocenylamino-propyl-piperazinyl-propyl-3-O-acetylursolamide	130A, 132A, 132A, 26A	ARG, GLU, GLU, SER	Immunoglobulin-like domain (19-90), Interleukin-12 beta, central domain (126-216),
IL-23A	3-3-carbonyl-pyridine-5-22-diene-24-ethyl-cholesterol	168A	SER	No Domains
IL33	Lupeol-acetylsalicylate	167A	GLN	No Domains
IL-7	3-Benzenesulfonyloxygen-5-22-diene-24-ethyl-cholesterol	122A	LYS	No Domains
IL1B	28-Methyl-3-O-acetyloleanane	119A	VAL	Not within the domain
IL-16	Lupeol-acetylsalicylate	227A	LEU	PDZ domain (216-303)
IL-24	3-2-4-dinitrophenyl-5-22-diene-24-ethyl-cholesterol	119A	THR	No Domains
IL-15	28-Methyl-3-O-acetyloleanane	25A	PHE	No Domains
IL-28A	Lupeol-isonicotinate	79A, 80A	LEU, PHE	No Domains
IL-30	N-3-4-3-4-Hydroxybenzyl-amino-propyl-piperazinyl-propyl-3-O-acetylursolamine	186A, 187A, 190A	GLY, SER, GLN	No Domains
IL-32	Stigmasterol	122A	GLU	No Domains
IL-36A	3-Benzenesulfonyloxygen-5-22-diene-24-ethyl-cholesterol	29A	THR	No Domains
IL-13	28-Methoxyoleanolic-acid	32A	TRP	No Domains
IL-29	3-Trifluoroacetyloleanolicacid	171A, 174A, 175A	PHE, PHE, ARG	No Domains
IL-36B	Lupeol-acetylsalicylate	61A	MET	No Domains
IL-34	Lupeol-isonicotinate	150A	ASN	No Domains
IL-4	28-Methoxyoleanolic-acid	60A	SER	No Domains
IL-3	Lupeol-acetylsalicylate	32A	TRP	No Domains
IL-12A	3-2-4-dinitrophenyl-5-22-diene-24-ethyl-cholesterol	137A	GLU	No Domains
IL-21	Lupeol-acetylsalicylate	154A	SER	No Domains

IL-31	28-Methyl-3-O-acetyloleanane	122A	THR	No Domains
IL-17A	3-2-4-dinitrophenyl-5-22-diene-24-ethyl-cholesterol	43A	ARG	No Domains
IL18	28-Methyl-3-trifluoroacetyl-oleanane	119A	PHE	No Domains
IL-26	28-Methyl-3-trifluoroacetyl-oleanane	53A	LYS	No Domains
IL-20	Oleanolic-Acid	98A, 114A	TYR, ASN	No Domains
IL-2	28-Methyl-3-trifluoroacetyl-oleanane	103A	ARG	No Domains
IL-11	28-Methoxyoleanolic-acid	172A	ARG	No Domains
IL22	28-Methyl-3-trifluoroacetyl-oleanane	166A	GLU	No Domains
IL1A	Oleanolic-Acid	162A	GLU	Interleukin-1 propeptide (1-109)
IL-19	Lupeol-acetylsalicylate	52A, 49A	GLN, ASP	No Domains
IL-27B	Lupeol-isonicotinate	135A	VAL	Fibronectin type III (129-227)
IL6	Lupeol-acetylsalicylate	94A, 114A	LYS, LYS	No Domains
IL-9	28-Methoxyoleanolic-acid	21A	CYS	No Domains
IL-8	Lupeol-acetylsalicylate	40A, 43A	TYR, PRO	Chemokine interleukin-8-like domain (31-92)
IL-14	Lupeol-acetylsalicylate	60A	SER	No Domains